Laser-induced breakdown in argon at 0.35 μm: Theory and experiments

Guy M. Weyl and David Rosen
Physical Sciences Inc., Research Park, Andover, Massachusetts 01810
(Received 20 August 1984)

The physical processes leading to laser-induced breakdown of argon in the flux range $10^9 < I < 10^{12}$ W/cm^2 have been analyzed. A model has been developed to predict breakdown thresholds which includes multiphoton ionization of ground-state atoms and electron-impact excitation of $4s$ and $4p$ states of Ar followed by photoionization of these states. Important processes that occur when the electron concentration exceeds 10^{14} cm^{-3}, such as three-body recombination, dimer formation, dissociative recombination, photodissociation, and photoionization of the excited molecular and/or atomic species formed, have been included in a late-time breakdown model in order to determine the channels through which the laser energy is deposited in the gas. Experiments have been carried out with use of a frequency-tripled neodymium-doped yttrium-aluminum-garnet beam with 15-ns pulse length, yielding a breakdown threshold of 3×10^{10} W/cm^2 at $p=1$ atm in good agreement with model predictions. Comparison of theoretical thresholds and thresholds reported in the literature for pulse lengths in the range 0.4—500 ns is presented.

I. INTRODUCTION

When a high-power laser beam of intensity I interacts with a gas, electrons can be generated through two main mechanisms: direct multiphoton ionization (MPI) and electron-impact ionization. In the first process an atom or molecule of ionization energy ϵ_I absorbs n simultaneous photons of energy $h\nu$, subject to the condition $nh\nu \geq \epsilon_I$, and thereby becomes photoionized. The ionization rate varies as I^n and the electron density, for a constant intensity pulse, increases linearly with time. In the second process electrons gain energy from the laser field through inverse bremsstrahlung (IB) collisions with neutrals. The electrons can readily ionize the gas when their energy exceeds ϵ_I. At sufficiently high fields ionizing collisions will cause an electron cascade to occur with the electron density increasing exponentially with time. Cascade breakdown is the dominant mechanism at long wavelengths ($\lambda \geq 1$ μm) and moderate-to-high pressures when there are many electron-neutral collisions during the laser pulse.[1] As the wavelength is shortened below 1 μm, however, multiphoton effects are expected to play an increasingly important role in the breakdown process. Multiphoton ionization of the host gas and of low ionization potential impurities will generate the initial electrons from which a cascade can develop. Also, if a sufficient concentration of electrons is generated by MPI early enough in the pulse so as to affect the diffusion of electrons out of the focal volume—diffusion becomes "ambipolar" in nature as opposed to "free"—the breakdown thresholds will be significantly lowered especially in experiments with small focal spots where diffusion losses can be important.

Though microwave breakdown theory[1–4] has been successfully used to evaluate breakdown thresholds at wavelengths beyond 1 μm, where IB absorption is the dominant mechanism leading to cascade breakdown, data at visible and near-uv wavelengths are not so well understood. If electron-impact ionization were the dominant mechanism leading to gas breakdown, one would expect that the breakdown threshold for a given gas at a given pressure would scale inversely with the IB absorption coefficient, i.e., as $\{\lambda^3[1-\exp(-hc/\lambda kT)]\}^{-1}$, where T is the electron temperature during the cascade.[5] Buscher *et al.*[6] observed, however, by studying breakdown in the rare gases at four wavelengths ($\lambda=1.06$, 0.69, 0.53, and 0.35 μm), that the breakdown thresholds peaked in the middle of the visible spectrum. Though they gave no explanation for this wavelength behavior, it can be reasonably postulated as being due to the increasing importance at short wavelengths of multiphoton ionization of the ground state and of excited states of the rare-gas atoms.

We analyze in this paper the various processes leading to breakdown in argon at $\lambda=0.35$ μm at near atmospheric pressure in the intensity range 10^9–10^{12} W/cm^2. The broad features of the model have been presented in an earlier publication.[7] Electrons are generated in the early stages of the breakdown process by MPI, by photoionization of impurities in the gas, and by electron cascade. The cascade ionization rate is determined by a balance between the rate of energy gained by the electrons from the laser field through IB collisions with neutrals and the power lost through excitation and ionization collisions with neutrals. When the electron density is below 10^{13} cm^{-3}, electron-electron collisions are not frequent enough to make the electron distribution function Maxwellian. One must resort to the use of a quantum kinetic code in order to calculate the electron distribution function and determine the excitation and ionization rates. Such a computer simulation of laser-induced breakdown in argon at photon energies of $h\nu \leq 2.5$ eV and below ($\lambda > 5000$ Å) has been carried out by Friedland,[8] who numerically solved the quantum kinetic equation given by Phelps[9] and included the important process, first pointed out by Zel'dovich and Raizer,[10] of two-photon ionization of excited states of argon. We follow the same approach in this paper. Two-photon ionization of excited states are expected to play a

much more important role at 0.35 μm than at the longer wavelengths previously studied because the lowest-lying excited ($4s$) states of argon can readily be ionized at the fluxes considered here by absorption of two photons, while absorption of three photons are required for $\lambda > 0.6$ μm. When the electron concentration exceeds 10^{13} cm^{-3}, electron-electron collisions will tend to populate the tail of the electron distribution function and this has a dramatic effect on the cascade rate, the effective IB absorption coefficient, as we shall show in this paper, being a factor of roughly 2 larger than if electron-electron collisions had not been included in the model. This is due to the large increase with energy of the momentum-transfer cross section of electrons with Ar at energies above 0.3 eV.

We also analyze in this paper the various processes that occur in the late-time breakdown stage when the electron concentration n_e exceeds 10^{14} cm^{-3}. It is in this last stage that essentially all of the energy deposition in the gas occurs. This has not been done previously, to the authors's knowledge. One must include at high n_e the effect of electron collisions with excited states and the chemistry of electron recombination and argon dimer formation. We have done this in a somewhat simplified way by assuming a two-temperature (electron temperature and heavy temperature) model of the gas. Late-time chemistry will lead to several new channels for deposition of laser energy in the gas, the two most important being photodissociation of Ar_2 and photoionization of excited states of argon formed by three-body recombination of Ar^+ with electrons.

Breakdown in gases near atmospheric pressure for laser pulse durations longer than a nanosecond are observed as a visual flash,[1] corresponding to essentially total ionization in the focal volume. It is, therefore, of interest to carry out a realistic analysis of breakdown up to electron densities exceeding 10^{17} e^-/cm^3. We define in this paper the breakdown time as the time it takes the electron density to reach 10^{17} e^-/cm^3. Though this is a somewhat arbitrary criterion, it can be justified for practical purposes by the fact that the time for n_e to grow from 10^{17} e^-/cm^3 to a density corresponding to complete ionization is much shorter than the time for n_e to reach 10^{17} e^-/cm^3.

There have been several measurements of laser-induced breakdown of argon at 0.35 μm under near-atmospheric-pressure conditions and for pulse lengths spanning the 10^{-11}–10^{-6} s range.[6,7,11,12] It is clear from the data of Kracyuk and Pashinin[11] taken with a pulse length $\tau_p = 40$ ps that breakdown was dominated by multiphoton ionization of Ar. We have inferred from their data an MPI cross section and used it in our breakdown model since no direct measurement of this cross section has been carried out to date. The measurements of Buscher *et al.*[6] and Alcock *et al.*,[12] performed using a frequency-doubled ruby laser beam ($\lambda = 0.347$ μm) with essentially the same pulse length (10 and 20 ns, respectively), are in substantial agreement with each other but are inconsistent with the measurements (and model) of Weyl *et al.*,[7] who used an XeF laser ($\lambda = 0.352$ μm) with $\tau_p = 0.5$ μs and a frequency-tripled Nd:glass laser beam ($\lambda = 0.351$ μm) with $\tau_p = 0.4$ ns. We report here a new set of measurements carried out using a frequency-tripled Nd:YAG (neodymium-doped yttrium-aluminum-garnet) beam with $\tau_p = 15$ ns, obtaining a breakdown threshold that is an order of magnitude higher than the frequency-doubled ruby laser beam data. We compare in this paper the results of our theoretical model with the available data.

II. EARLY-TIME BREAKDOWN ANALYSIS FOR ARGON

The energy levels of argon are shown in Fig. 1. One sees from this figure that an electron must absorb four photons before it has enough energy to excite the $4s$ states (Ar^*) at 11.6 eV and $4p$ states (Ar^{**}) between 13.2 and 13.6 eV. Photoionization of Ar^{**} by absorption of one photon is possible. Two photons, however, are required to photoionize Ar^*, while photoionization of the ground state requires simultaneous absorption of five photons.

We model the physical processes leading to breakdown in argon at early time through the following set of reactions.

Direct multiphoton ionization:

$$X(\text{impurity}) + mh\nu \rightarrow X^+ + e^- , \tag{1}$$

$$\text{Ar} + 5h\nu \rightarrow \text{Ar}^+ + e^- . \tag{2}$$

Electron inverse bremsstrahlung absorption:

$$e^-(\epsilon) + \text{Ar} + h\nu \rightarrow e^-(\epsilon + h\nu) + \text{Ar} . \tag{3}$$

Electron-impact excitation of Ar:

$$e^-(\epsilon) + \text{Ar} \rightarrow \text{Ar}^* + e^-(\epsilon - 11.6\ \text{eV}), \quad \epsilon > 11.6\ \text{eV} \tag{4}$$

$$e^-(\epsilon) + \text{Ar} \rightarrow \text{Ar}^{**} + e^-(\epsilon - 13.2\ \text{eV}), \quad \epsilon > 13.2\ \text{eV} . \tag{5}$$

Photoionization of the excited states formed:

$$\text{Ar}^* + 2h\nu \rightarrow \text{Ar}^+ + e^- , \tag{6}$$

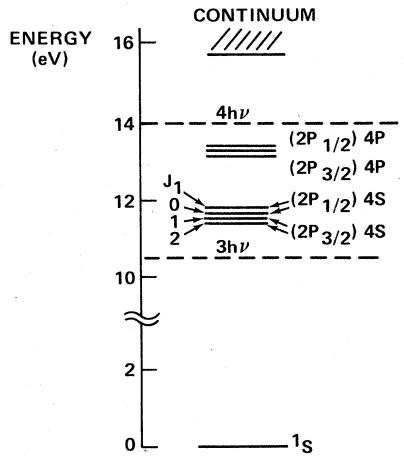

FIG. 1. Energy levels in argon.

$$Ar^{**}+h\nu \rightarrow Ar^{+}+e^{-} . \quad (7)$$

We analyze each of the above processes below.

A. Direct multiphoton ionization

The probability that argon will absorb m ($=5$) photons to become ionized can be calculated quantum mechanically using mth-order perturbation theory. One finds that the lifetime varies as I^{-m}. A review of the work done until 1976 can be found in Ref. 13. The difficulty in deriving an MPI cross section is that one has to perform a multiple summation over intermediate states and that subtle interference effects between terms can occur. Also, the wave functions required for calculating the matrix elements are not that well known except for the simplest atoms. Calculated and measured lifetimes can differ by many orders of magnitude.[13] There has been no theoretical calculation for multiphoton ionization in argon at 0.35-μm wavelength. Experimental studies of breakdown in argon at doubled ruby laser frequency ($\lambda/2=3470$ Å) in the pressure range 400—5000 Torr were carried out by Krasyuk and Pashinin,[11] with $3\times10^{-11}<\tau_p<5\times10^{-11}$ s. They defined the threshold for breakdown as that intensity which produced a faint glow to the eye in the focal region. Their threshold curve is practically independent of p and is consistent with the scaling $I\propto p^{-1/5}$ as one would expect for an MPI threshold corresponding to a fixed number of ions in the focal volume. The fact that the threshold did not correspond to a sharp breakdown transition is also an indication that breakdown was not associated with an electron cascade. We derive in Appendix A from their data an MPI cross section

$$Q_5=1\times10^{-147}\ \mathrm{cm^{10}s^4} . \quad (8)$$

The multiphoton-ionization rate depends strongly on beam temporal coherence.[1,13,14] It is reasonable to assume that the 30-ps pulse duration experiments in Ref. 11 used a coherent beam, since the 30-ps pulses were obtained by modelocking, i.e., having a definite phase relationship between the many modes that are oscillating simultaneously. In experiments carried out with longer pulses ($\tau_p>10^{-8}$ s), however, the presence of many longitudinal modes will result in the laser beams being temporally incoherent.[15] The cross section would accordingly be larger by a factor of $m!$ ($=120$) for the longer pulses,[1,13,14] i.e.,

$$Q_5(\text{incoherent})\cong1\times10^{-145}\ \mathrm{cm^{10}s^4} . \quad (9)$$

B. Electron-neutral inverse bremsstrahlung absorption at 0.35 μm

The inverse bremsstrahlung absorption cross section is usually derived by calculating bremsstrahlung emission and using the principle of detailed balance.[16] We are concerned with electrons whose average energy is of the order of or smaller than $h\nu$. A proper treatment of the emission and absorption must be quantum mechanical. There is some confusion in the literature on the proper absorption cross section to use. The IB absorption coefficient per unit electron and neutral density that we have used is given by

$$K_a=\frac{4\pi e^2}{3mc\omega^2}\left[\frac{2(\epsilon+h\nu)}{m}\right]^{1/2}\times\left[\frac{\epsilon+h\nu}{h\nu}\sigma_m(\epsilon)+\frac{\epsilon}{h\nu}\sigma_m(\epsilon+h\nu)\right] , \quad (10)$$

where e and m are the electron charge and mass, respectively, c is the speed of light, ω the angular frequency, ϵ the electron energy *before* absorption of a photon, and σ_m the momentum-transfer cross section for electrons colliding with neutrals. Equation (10) was derived by Dalgarno and Lane,[17] who solved the quantum-mechanical scattering problem in an electromagnetic field of angular frequency ω by performing a partial-wave analysis and keeping only the contributions from s and p waves. It differs from the expression given by Zel'dovich and Raizer[16] and by Kroll and Watson[18] where the last bracket is replaced by $2(\epsilon+h\nu)\sigma_m(\epsilon+h\nu)/h\nu$ and also differs from an expression used by Phelps[9] where the last bracket is replaced by $2(\epsilon+h\nu/2)\sigma_m(\epsilon+h\nu/2)/h\nu$. Note, however, that Dalgarno and Lane's expression for K_a reduces to that of Phelps when σ_m is independent of ϵ and that all expressions are equivalent when $h\nu\ll\epsilon$. Equation (10) can be written as

$$K_a=6.0\times10^{-25}\lambda^2(\mu\mathrm{m})(\epsilon+h\nu)^{1/2}\times\left[\left[1+\frac{\epsilon}{h\nu}\right]\sigma_m(\epsilon)+\frac{\epsilon}{h\nu}\sigma_m(\epsilon+h\nu)\right] ,$$

where ϵ and $h\nu$ are expressed in eV and σ_m in cm^2. K_a has units of cm^5. Electrons can also emit photons when colliding with neutrals. The stimulated emission coefficient K_e, obtained from detailed balance, is

$$K_e(\epsilon)=K_a(\epsilon-h\nu)\left[\frac{\epsilon-h\nu}{\epsilon}\right]^{1/2} ,$$

when $\epsilon>h\nu$ and $K_e(\epsilon)=0$ when $\epsilon\leq h\nu$. If one has a Maxwell-Boltzmann distribution of electrons corresponding to a temperature T, then the *net* absorption cross section averaged over the distribution function $f(\epsilon)$ is

$$\overline{K}=\int_0^\infty f(\epsilon)d\epsilon[K_a(\epsilon)-K_e(\epsilon)] =(1-e^{-h\nu/kT})\int_0^\infty f(\epsilon)K_a(\epsilon)d\epsilon . \quad (11)$$

C. Electron-impact excitation of argon

The inelastic cross sections for excitation of electronic states of argon have been reviewed by Eggarter.[19] Jacob and Mangano[20] have used the cross sections suggested by Eggarter to calculate, by use of a Boltzmann code, the first Townsend ionization coefficient in argon and found that these had to be reduced by a factor of ~2 in order to obtain agreement with the data. The cross sections that gave the best fit were 10% larger than those measured by Shaper and Scheibner.[21] These cross sections, however, represent excitation of both $4s$ and $4p$ states of argon. Since it is important, in order to model breakdown at 0.35

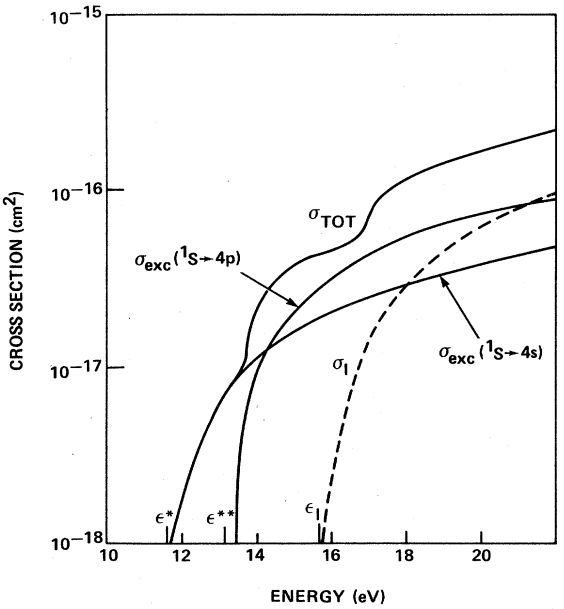

FIG. 2. Electron inelastic cross sections in argon.

μm, to break up the cross section into excitation of the $4s$ and $4p$ states separately, we have used the cross sections furnished by Center[22] and adjusted them in order to fit the first Townsend ionization coefficient data. The adjustment factor was found to be 0.8. The cross sections have been plotted in Fig. 2. The sum of the cross sections is in good agreement with the data of Shaper and Scheibner[21] at energies below 13.5 eV and is in good agreement with Eggarter's total cross-section estimate[20] above 14 eV.

D. Photoionization of excited states of argon

The $4p$ states and higher-lying states are within $h\nu$ of the ionization continuum and can be photoionized by absorbing one photon. One estimates the cross section σ_{phi} to be of the order of 10^{-17} cm^2 so that the lifetime of these states in the laser beam is

$$\tau=\frac{h\nu}{\sigma_{\text{phi}}I}\cong 5\times 10^{-2}I^{-1}\text{ s},$$

where I is in W/cm^2. The radiative lifetime for allowed transitions to the ground state is 3×10^{-9} s or longer[23] so that at fluxes $I>10^7$ W/cm^2 photoionization is more probable than radiative decay. Also, any radiation to the ground state is strongly reabsorbed, resulting in trapping of the radiation. The effective lifetime may be as long as a few microseconds, depending on the focal spot size and the operating pressure. Radiative decay to the lower-lying $4s$ state, resulting in radiation that is not trapped, occurs with lifetimes $\tau>5\times 10^{-8}$ s. We can therefore assume, in our model for breakdown, that at fluxes larger than 10^6–10^7 W/cm^2 the excitation of the $4p$ and higher-lying

TABLE I. Contribution of various levels to photoionization cross section of excited states in argon.

Lower level m	E_m (eV)	Interm. level j	$h\nu-E_j+E_l$ (eV)	f_{mj}	σ_{phi} (10^{-16} cm^2)	$\frac{\sigma_{\text{phi}}f_{mj}}{(h\nu-E_j+E_l)^2}$ 10^{-18} (cm/eV)^2
$4s(\frac{3}{2})^0$	11.544	$4p(\frac{1}{2})$	2.15	0.212	0.16	0.714
		$4p(\frac{5}{2})$	1.98	0.366	0.141	1.31
		$4p(\frac{3}{2})$	1.89	0.274	0.126	0.971
		$6p(\frac{3}{2})$	0.0247	5.5×10^{-4}	0.0042	0.37
$4s(\frac{3}{2})^0$	11.620	$4p'(\frac{5}{2})$	2.04	0.413	0.138	1.36
		$4p(\frac{3}{2})$	1.98	0.273	0.129	0.897
		$4p(\frac{1}{2})$	1.86	0.121	0.112	0.39
		$6p(\frac{1}{2})$	0.075	5.3×10^{-4}	0.0037	0.03
$4s'(\frac{1}{2})^0$	11.72	$4p'(\frac{3}{2})$	1.95	0.56	0.11	1.6
		$4p'(\frac{1}{2})$	1.90	0.341	0.11	1.0
		$6p(\frac{3}{2})$	0.034	7.4×10^{-4}	0.002	0.12
$4s'(\frac{1}{2})$	11.82	$4p'(\frac{3}{2})$	2.06	0.160	0.11	0.42
		$4p'(\frac{3}{2})$	2.04	0.431	0.11	1.1
		$4p'(\frac{1}{2})$	2.01	0.172	0.11	0.45
		$4p'(\frac{1}{2})$	1.86	0.133	0.080	0.33
		$7p(\frac{1}{2})$	0.0424	3.4×10^{-4}	0.0013	0.024

states is immediately followed by photoionization.

The $4s$ states in the energy range 11.6—11.8 eV above the ground state (see Fig. 1) require the simultaneous absorption of two 3.5-eV photons in order for ionization to occur. We estimate, in Appendix B, using second-order perturbation theory, the probability per unit time for two-photon ionization of the $4s$ states. Neglecting cross terms in the sum over intermediate states j and considering only the most important transitions, we find (I in W/cm^2 and energies in eV)

$$W_{ml}=\frac{5\times10^5 I^2}{(h\nu)^2}\sum_j \frac{\sigma^j_{\rm phi} f_{mj}}{(h\nu-\epsilon_{jl})^2}\ {\rm s}^{-1}$$

$$\cong 1.1\times10^{-13} I^2\ , \tag{12}$$

where m refers to the initial (s) state, l refers to the final state in the continuum, $\sigma^j_{\rm phi}$ is the photoionization cross section (in cm^2) of state j, and f_{mj} is the f number for the transition $m\rightarrow j$. In the last step we evaluated the sum for the most important terms shown in Table I. We see from Eq. (10) that when $I>10^{11}$ W/cm^2, $W_{ml}\geq 10^9$ s^{-1}. Two-photon ionization of the $4s$ states should therefore play an important role in the breakdown process for $I>10^{11}$ W/cm^2 and $\tau_p>10^{-8}$ s.

E. Early-time cascade development

The early-time cascade development can be analyzed by writing rate equations for reactions (1)—(7). Let n, n^*, and n_e be the density of Ar, Ar*, and electrons. We will have the following rate equations for the formation of electrons and $4s$ excited states:

$$\frac{dn_e}{dt}=W_{ml}n^*+k_2 n_e n+S\ , \tag{13}$$

$$\frac{dn^*}{dt}=k_1 n_e n-W_{ml}n^*\ , \tag{14}$$

where k_1 is the rate of formation of Ar* by reaction (4), k_2 is the rate of formation of Ar** by reaction (5), and we assumed that Ar** is immediately photoionized by reaction (7). From Eq. (12) we have $W_{ml}=AI^2$ with $A=1.1\times10^{-13}$ s^{-1}(W/cm^2)$^{-2}$. The term S represents sources and sinks of electrons, the source being multiphoton ionization of Ar [reaction (2)] and multiphoton ionization of impurities. The sink of electrons would include a diffusion loss term of the form $-(\mathscr{D}/\Lambda^2)n_e$, where $\mathscr{D}$ is the electron diffusion coefficient and Λ is a scale size of the order of the beam radius. We solve Eqs. (13) and (14) with the neglect of diffusion losses, with the initial condition $n_e=n^*=0$, and $\dot{n}_e=S$. The result is found to be, after some algebra,

$$n_e=\frac{S}{(k_1+k_2)n}(a_+e^{\alpha_+ t}+a_-e^{\alpha_- t}-1) \tag{15}$$

with

$$a_\pm=\frac{(k_1+k_2)n-\alpha_\mp}{\alpha_\pm-\alpha_\mp}$$

and

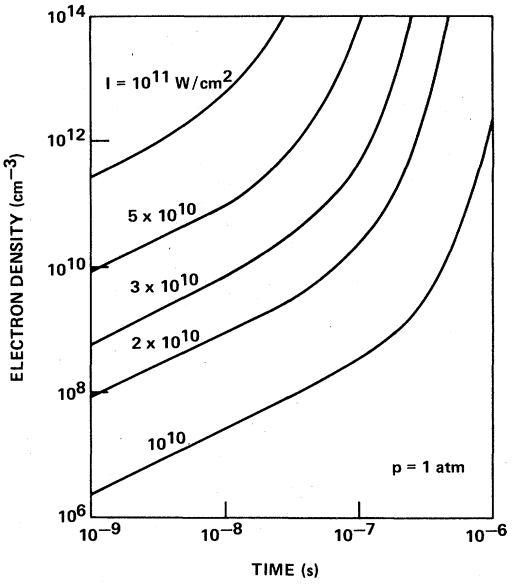

FIG. 3. Early-time electron growth, argon at standard density.

$$\alpha_\pm=\frac{-W_{ml}\pm[W_{ml}^2+4W_{ml}(k_1+k_2)n]^{1/2}}{2}\ .$$

The growth of n_e versus t given by Eq. (15) is shown in Fig. 3. The exponential growth at late times is due to the first term in Eq. (15). Curves of constant α^+, shown in Fig. 4, indicate that α^+ (or breakdown time) will be a function of Ip^m, where $0.5<m<1$, over the range of parameters considered. The rates k_1 and k, used in our calculations, were derived from a quantum kinetic code written by Morgan at the Joint Institute for Laboratory Astro-

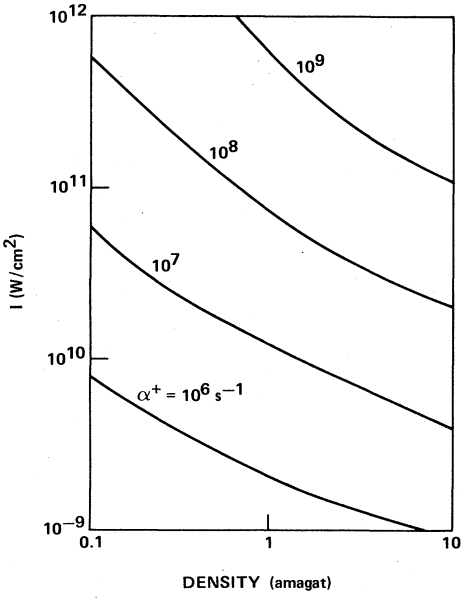

FIG. 4. Cascade rate coefficient α^+ as a function of laser intensity for early-time cascade growth in argon, $h\nu=3.5$ eV.

physics. We used in the code the cross sections for excitation that were described previously. The momentum-transfer cross section (σ_m) was taken from the data of Frost and Phelps[24] and the ionization cross section σ_I, plotted in Fig. 2, was taken from the data of Rapp and Englander-Golden.[25] The IB cross section used was that derived by Dalgarno and Lane,[17] given by Eq. (10). The excitation rates obtained in the intensity range 10^{10}—3×10^{11} W/cm^2 could be fitted by the relations

$$k_1 = 5\times10^{-23} I \text{ cm}^3/\text{s} , \tag{16}$$

$$k_2 = \frac{2.5\times10^{-13}(I/10^{10})^{1.28}}{1+\left[\frac{I}{10^{10}}\right]^{0.28}} \text{ cm}^3/\text{s} , \tag{17}$$

where I is in W/cm^2.

The code results indicate that most of the energy absorbed by the electrons is transferred to the neutrals through inelastic collision resulting in excitation of the $4s$ and $4p$ states. At a laser flux of 10^{10} W/cm^2 only 25% of the absorbed energy goes into heating the gas through momentum-transfer collisions, and this fraction decreases as the intensity is increased above 10^{10} W/cm^2. Therefore, at high laser intensity [when $W_{ml} \gg 4(k_1+k_2)n$] the cascade growth rate α^+ will be nearly equal to $(k_1+k_2)n$ and will be proportional to the IB absorption coefficient $\overline{K}$.

F. Effect of electron-electron collisions

As the electron density increases, electron-electron collisions become important and tend to make the electron distribution Maxwellian. We can estimate the electron density above which electron-electron collisions become important by comparing the electron equilibration time t_{ee} at an average electron energy $\bar{\epsilon}$ with the electron heating time t_H. We have $t_{ee}=0.26T_e^{3/2}(n_e \ln\Lambda)$ where T_e is in K, n_e is in cm^{-3}, and $\ln\Lambda$ is the Coulomb logarithm.[26] The excitation time is, from Eqs. (16) and (17), $t_{exc} = [(k_1+k_2)n]^{-1} \cong 6\times10^{-8}(10^{10}/I)p^{-1}$, where I is in W/cm^2 and p is in atm. The heating time is smaller than the excitation time by the ratio $\bar{\epsilon}/\epsilon^* \cong 1.2$ eV/11.6 eV$\approx$0.1. Therefore, in order that $t_{ee} \ll t_H$, we must have $n_e \gg (4\times10^7 T_e^{3/2}/\ln\Lambda)p(I/10^{10}) \simeq 10^{13}p(I/10^{10})$, where in the last step we set $T_e = 10\,000$ K and $\ln\Lambda \cong 6$. The effect of electron-electron collisions on the electron distribution and on the heating rate (or effective absorption coefficient) is dramatic. We show in Fig. 5 two electron distribution functions obtained with and without electron-electron collisions, when $n_e = 10^{14}$ cm^{-3}. The heating rate when electron-electron collisions are included is two to three times larger than when they are not. This is due to the fact that IB absorption by electrons in the tail of the distribution function is much larger than at the peak. When electron-electron collisions are important, transport of electrons to the tail occurs through these collisions; in the absence of electron-electron collisions, however, transport occurs through absorption of photons, and absorption at moderate-to-low electron energies forms a bottleneck for the heating process.

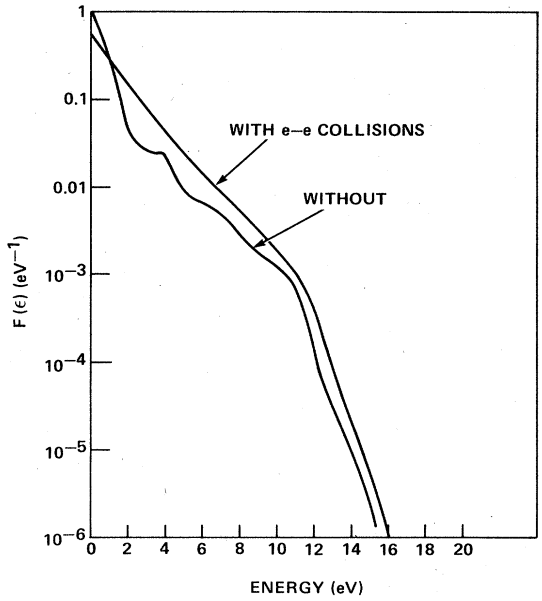

FIG. 5. Effect of electron-electron collisions on the distribution function of electrons.

III. LATE-TIME BREAKDOWN STAGE

When the electron density exceeds $\sim10^{14}$ cm^{-3} many more processes must be included in order to adequately model the mechanisms for energy absorption and free-electron generation. We saw in Sec. II F that, for our conditions of interest ($I \cong 10^{10}$—10^{11} W/cm^2, $p \cong 1$ atm), the electrons will have a Maxwellian distribution when $n_e \geq 10^{14}$ cm^{-3}. We can therefore model the late-time breakdown by assuming that we have a two-temperature gas. Let T_e be the electron temperature, $\bar{\epsilon}$ ($=\frac{3}{2}kT_e$) the average electron energy, and T_g the heavy particle temperature. The rates for reactions (4) and (5) are obtained by a suitable averaging of the cross sections over the distribution function. Electron-ion recombination must be included in the model when the electron density gets to be large enough. Also, electron-impact ionization of excited states becomes important as the population of excited states builds up. We must, therefore, add to the series of reactions (1)—(7) the following reactions:

$$\text{Ar}^+ + 2\text{Ar} \rightarrow \text{Ar}_2^+ + \text{Ar} , \tag{18}$$

$$\text{Ar}_2^+ + e^- \rightarrow \text{Ar} + \text{Ar}^{**} , \tag{19}$$

$$\text{Ar}^* + e^- \rightarrow \text{Ar}^{**} + e^- , \tag{20}$$

$$\text{Ar}^* + e^- \rightarrow \text{Ar}^+ + 2e^- , \tag{21}$$

$$e^- + e^- + \text{Ar}^+ \rightarrow \text{Ar}^{**} + e^- . \tag{22}$$

Reaction (18) is very fast at atmospheric pressure, having a rate coefficient of 3×10^{-31} cm^6/s. It leads to the formation of ion dimers which very rapidly recombine with electrons through reaction (19). Reaction (19) has a rate coefficient of $9.1\times10^{-7}(300/T_e)^{0.61}$ cm^3/s, where T_e is in K, and leads to excited argon atoms principally in the $4p$ state.[27]

We expect, at the high laser fluxes that we are considering, that the photodissociation of Ar_2^+ will be faster than reaction (19). The potential-energy curves for Ar_2^+ and other excited states of the Ar_2 dimer have been derived by Lorentz and Olsen.[28] The binding energy of Ar_2^+ is 1.24 eV. Photodissociation will occur through the channel:

$$Ar_2^+(^2\Sigma_u^+)+h\nu\rightarrow Ar_2^+(^2\Sigma_g^+)\rightarrow Ar+Ar^+ . \quad (23)$$

We therefore combine reactions (18) and (23) into the following overall reaction which results in heating of the gas:

$$Ar^+ + 2Ar + h\nu \rightarrow 2Ar + Ar^+ . \quad (18')$$

Since the rate-limiting step for (18′) is reaction (18), we shall use the rate for reaction (18) in reaction (18′). In a similar way we replace reaction (20) by

$$Ar^* + e^- + h\nu \rightarrow Ar^+ + 2e^- . \quad (20')$$

The three-body recombination reaction (22) is extremely important in the late stages of the breakdown processes since it leads to the formation of excited states of argon which are rapidly photoionized. It leads to an effective plasma absorption coefficient larger than that due to electron-ion and electron-neutral inverse bremsstrahlung in two-body collisions. We replace reaction (22) by

$$h\nu + e^- + e^- + Ar^+ \rightarrow Ar^+ + 2e^- . \quad (22')$$

The three-body recombination rate for reaction (22) has been studied by Gurevich and Pitaevskii[29] and by Bates *et al.*[30]

We model the breakdown by adding to the inverse bremsstrahlung absorption by the electrons the effects of reactions (18′), (20′), (21), and (22′). We have three species—electrons, Ar, and Ar*—and two temperatures—T_e and T. Let x_e, x, and x^* be the densities of electrons, Ar, and Ar* normalized to the initial gas density n. The five equations describing the breakdown at late times are the following.

Species conservation:

$$x_e + x + x^* = 1 . \quad (24)$$

Rate of growth of electrons and Ar*:

$$\frac{dx_e}{dt} = \nu' x_e x^* + W_{ml} x^* + \nu^{**} x_e x , \quad (25)$$

$$\frac{dx^*}{dt} = \nu^* x_e x - W_{ml} x^* - \nu' x_e x^* . \quad (26)$$

Energy equation for electrons and excited states:

$$\frac{d}{dt}[(\bar{\epsilon}+\epsilon_I)x_e + \epsilon^* x^*] = [(\bar{K}_{en} x_e x + \bar{K}_{ei} x_e^2) n\Phi + x_e(\nu' + \nu^* x^* + \nu^{**} x) + 2W_{ml} x^* - \frac{2m}{M}\nu_m x_e(\bar{\epsilon} - \tfrac{3}{2}kT) + \mu x_e^3]h\nu . \quad (27)$$

Energy equation for the heavy particles:

$$\tfrac{3}{2}k\frac{d}{dt}T = \frac{2m}{M}\nu_m(\bar{\epsilon} - \tfrac{3}{2}kT)x_e + (k_R x_e x^2 n^2)h\nu . \quad (28)$$

In the above, ν^*, ν^{**}, and ν' are the excitation rates corresponding to reactions (4), (5), and (20), ϵ_I (=15.755 eV) is the ionization potential of argon, $\bar{K}_{en}$ and $\bar{K}_{ei}$ are the inverse bremsstrahlung absorption coefficients for electron-neutral and electron-ion collisions averaged over a Boltzmann distribution of electrons, ν_m is the momentum-transfer collision frequency between electrons and heavy particles, μ is the rate corresponding to reaction (22), and k_R the rate coefficient for reaction (18). Φ ($=I/h\nu$) is the photon flux in units of (area×time)$^{-1}$. Following Zel'dovich and Raizer,[31] we approximate the excitation cross section near threshold by $\sigma_{exc}(\epsilon) = C(\epsilon - \epsilon_{th})$ for $\epsilon > \epsilon_{th}$. After averaging over a Maxwellian distribution we obtain an excitation rate

$$\nu_{exc} = 3.23\times 10^7 nC\bar{\epsilon}^{3/2}\left[\frac{3}{2}\frac{\epsilon_{th}}{\bar{\epsilon}} + 2\right] \times \exp\left[-\frac{3}{2}\frac{\epsilon_{th}}{\bar{\epsilon}}\right] \text{ s}^{-1} \quad (29)$$

where C is in cm^2/eV, n in cm^{-3}, and $\bar{\epsilon}$ in eV. We use for argon $C = 10^{-17}$ cm^2/eV and obtain ν^*, ν^{**}, and ν' by letting ϵ_{th} be ϵ^*, ϵ^{**}, and $\epsilon^{**} - \epsilon^*$, respectively.

$\bar{K}_{en}$ is obtained from Eq. (11) by taking the average of $K_a\{1 - \exp[-(2h\nu/3\epsilon)]\}$ over a Boltzmann distribution of ϵ. $\bar{K}_{ei}$ is the electron-ion IB absorption coefficient per unit electron and ion density, corrected for stimulated emission, given by[32]

$$\bar{K}_{ei} = \frac{4}{3}\left[\frac{2\pi}{3mkT_e}\right]^{1/2}\frac{Z^2e^6}{hc\nu^3 m} n_e^2(1 - e^{-h\nu/kT_e})\bar{G} . \quad (30)$$

For the conditions of interest in this paper ($h\nu/kT_e \cong 1$–2), we can use a Gaunt factor $\bar{G} \cong 1.2$. Expression (28) can be rewritten as a function of $\bar{\epsilon}$,

$$\bar{K}_{ei} = \frac{3.5\times 10^{-37}}{\bar{\epsilon}^{1/2}(h\nu)^3}\left[1 - \exp\left[-\frac{3}{2}\frac{h\nu}{\bar{\epsilon}}\right]\right] \text{ cm}^5 , \quad (31)$$

where $h\nu$ and $\bar{\epsilon}$ are expressed in eV.

The collision frequency for momentum transfer, ν_m, has contributions due to electron-neutral and electron-ion collisions. We have

$$\nu_m = (x + x^*)\nu_a + x_e\nu_e , \quad (32)$$

where

$$\nu_a = n\left\langle\left[\frac{2\epsilon}{m}\right]^{1/2}\sigma_m(\epsilon)\right\rangle = 4.84\times 10^7 n\langle\epsilon^{1/2}\sigma_m(\epsilon)\rangle \text{ s}^{-1} \quad (33)$$

and ν_e is the inverse of the electron-electron equilibration time τ_{ee} discussed earlier.

The three-body recombination rate is[32]

$$\mu = \frac{5.6\times 10^{-26} n_e \Lambda}{(\bar{\epsilon})^{9/2}} \text{ cm}^3/\text{s} , \quad (34)$$

where Λ is a Coulomb logarithm of a special kind of order unity. At low laser fluxes and high electron densities three-body recombination can maintain local thermo-

dynamic equilibrium for the highly excited states. It can be shown,[33] by using a hydrogenic approximation for the excited states of Ar lying within $h\nu$ of the ionization continuum, that the total absorption coefficient, combining free-free and bound-free transitions, is $\overline{K}_{ei}e^{h\nu/kT_e}$, with $\overline{K}_{ei}$ given by Eq. (28). At high laser fluxes, where significant depletion of the population of excited states by photoionization occurs, the absorption coefficient is decreased. In order to find out at which n_e and I three-body recombination rates and photoionization rates are comparable, we equate power absorbed from the laser field ($\overline{K}_{ei}e^{h\nu/kT_e}n_e^2 I$) with the rate of recombination (μn_e^2) times the photon energy ($h\nu$). Using Eqs. (29) and (32) and expressing I in W/cm^2 and n_e in cm^{-3}, we find

$$\frac{I}{n_e}=2.6\times10^{-8}\left[\frac{h\nu}{\overline{\epsilon}}\right]^4(e^{3h\nu/2\overline{\epsilon}}-1)^{-1}. \quad (35)$$

The right-hand side of Eq. (35) has a maximum when $h\nu/\overline{\epsilon}=2.6$. Letting $n_e=10^{17}$ cm^{-3}, $h\nu=3.5$ eV, and $\overline{\epsilon}=1.35$ eV, we obtain $I=2.5\times10^9$ W/cm^2. We thus see that at the fluxes that we are considering ($I>10^9$ W/cm^2), it is a valid assumption during most of the breakdown process to treat bound-free absorption through reaction (22′).

The system of differential equations (25)—(28), subject to the constraint given by Eq. (24), was numerically integrated. The initial conditions were $x_e=10^{-7}$, $x^*=x^{**}=0$. The initial electron concentration was purposely chosen lower than the minimum value for which the late-time breakdown model is valid in order to allow the population of excited states to build up. The results for the case $p=1$ atm, $I=10^{10}$ W/cm^2 are shown in Figs. 6—9. The origin of time was taken as the time at which $x_e=10^{-6}$ ($n_e=2.5\times10^{13}$ cm^{-3}). The duration of the late-time breakdown stage is calculated to be $\sim$600 ns. The gas temperature and electron temperature remain constant during most of the induction time to breakdown (see Fig. 6). The buildup of the electron and excited-state argon population is shown in Fig. 7. The absorption coefficients due to the various absorption mechanisms are shown in Fig. 8. The two most important absorption mechanisms during most of the delay time to breakdown are electron-neutral inverse bremsstrahlung and photodissociation of the dimer Ar_2^+, the first mechanism being the one that determines the time evolution of the cascade. Most of the energy is deposited into the gas in the very last stages of the breakdown, and the absorption mechanisms, in order of importance, are photoionization of Ar** formed either by the three-body recombination reaction (22) or by electron-impact excitation on Ar*,

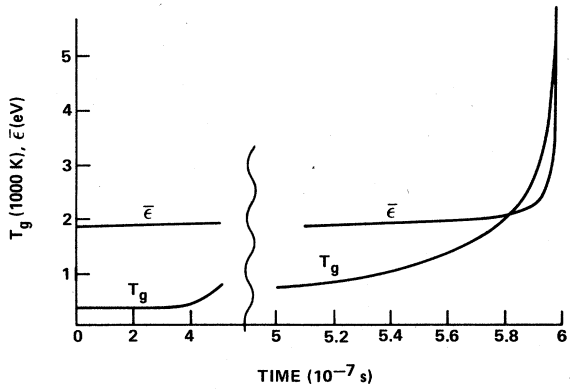

FIG. 6. Electron energy and gas temperature during late-time breakdown stage, $n=1$ amagat, $I=10^{10}$ W/cm^2.

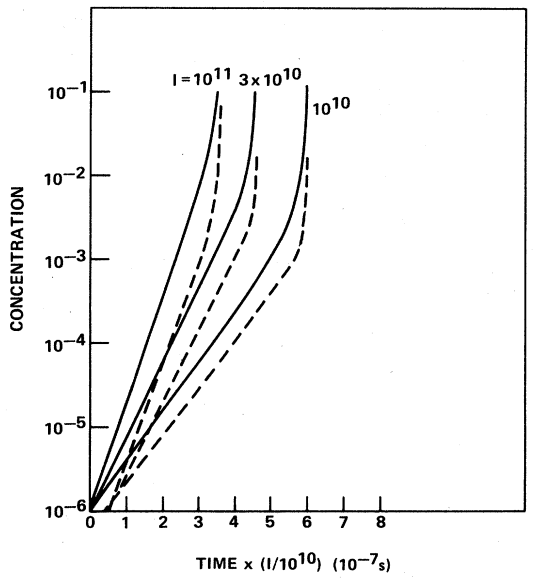

FIG. 7. Growth of electron concentration x_e (——) and first excited-state concentration x^* (— — —) in the late-time breakdown stage. I is the intensity in W/cm^2.

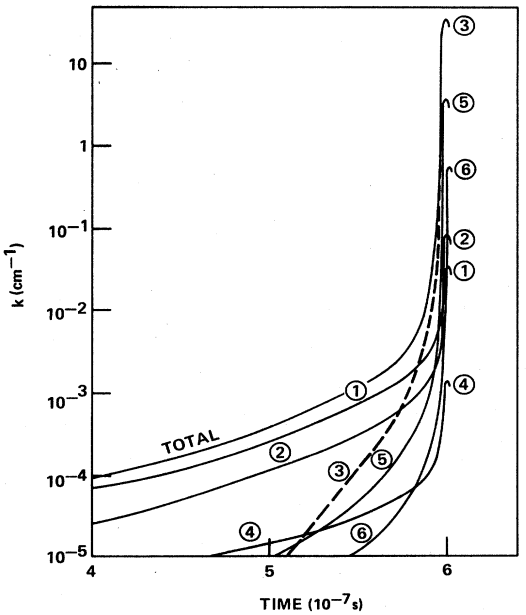

FIG. 8. Various absorption mechanisms in argon for $p=1$ atm, $I=10^{10}$ W/cm^2. (1) $Ar_2^*+h\nu\rightarrow Ar^*+Ar$, (2) electron-neutral IB, (3) $e^-+e^-+Ar^+ +h\nu\rightarrow e^-+e^-+Ar^+$, (4) $Ar^*+2h\nu\rightarrow Ar^+ +e$, (5) $Ar^*+e^-+h\nu\rightarrow Ar^{**}+e^-+h\nu \rightarrow Ar^+ +2e^-$, (6) electron-ion IB.

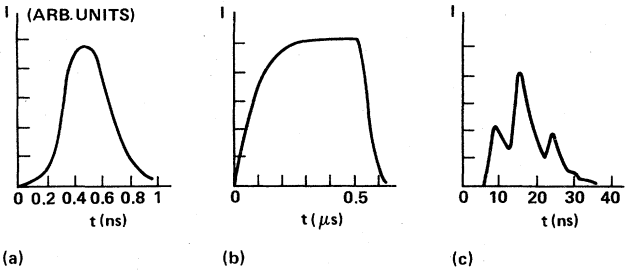

FIG. 9. Temporal profiles of laser pulses. (a) University of Rochester frequency-tripled Nd:glass laser beam, $\lambda=351$ nm; (b) XeF laser, $\lambda=353$ nm; (c) Massachusetts Institute of Technology—National Science Foundation frequency-tripled Nd:YAG beam, $\lambda=355$ nm.

electron-ion inverse bremsstrahlung, and electron-neutral inverse bremsstrahlung. For the case studied, the absorption coefficient reaches a maximum of 30 cm^{-1} at $t=0.6$ μs and decreases thereafter with increasing electron temperature. It is interesting to note that the electron-ion inverse bremsstrahlung absorption coefficient peaks at a value of 0.6 cm^{-1}, i.e., is 50 times lower than the recombination absorption.

Calculation of electron growth was carried out at a series of laser intensities ranging from 10^9 to 10^{11} W/cm^2. We show in Fig. 7 the growth with time of x_e and x^* at the three fluxes 10^{10}, 3×10^{10}, and 10^{11} W/cm^2. The ratio x^*/x_e remains constant over many e-folding times up to electron concentrations as high as 0.1. The ratio is determined by the balance between electron excitation (and deexcitation) and two-photon ionization of the $4s$ states. At the lower flux shown ($I=10^{10}$ W/cm^2) the two-photon-ionization time is long (10^{-7} s) as compared to the electron e-folding time and the ratio is large ($x^*/x_e=0.6$). At high fluxes ($I\cong10^{11}$ W/cm^2), where the population of $4s$ states is depleted on a time scale (10^{-9} s) shorter than the electron-cascade time, the ratio is small ($x^*/x_e=0.1$). If we had not included photoionization of the $4s$ states in our breakdown model, the ratio x^*/x_e would be equal to the ratio ν^*/ν^{**} (since $\nu_i\ll\nu^{**}$), i.e., approximately 2 over the range of intensities shown [see Eqs. (16) and (17)]. The average electron energy $\bar{\epsilon}$ was found to increase slightly with increasing intensity (from $\bar{\epsilon}=1.4$ to $\bar{\epsilon}=2.5$ eV as I was varied from 10^9 to 10^{11} W/cm^2).

A study of the sensitivity of the breakdown time to the value of W_{ml} was carried out. The effect of W_{ml} on breakdown time is the largest at the lowest fluxes considered. Increasing W_{ml} by a factor of 10 at $I=10^{10}$ W/cm^2 reduced the duration of the late-time breakdown stage by 30% ($\tau_{br}\cong4\times10^{-7}$ s instead of 6×10^{-7} s), while making $W_{ml}=0$ would increase the time by a factor of 2.

IV. COMPARISON WITH EXPERIMENTS

We apply the results of the early- and late-time breakdown models to the experimental conditions under which breakdown has been observed. Two sets of experiments have been carried out under practically identical conditions ($p\sim1$ atm, doubled ruby laser frequency $\lambda=0.347$ μm, $\tau_p=20$ and 8 ns) by Alcock *et al.*[12] and by Buscher *et al.*[6] As was reported earlier,[7] we carried out measurements at shorter pulse times ($\tau_p=0.4$ ns) using a frequency-tripled Nd:glass laser beam ($\lambda=0.3513$ μm) and at longer pulse times ($\tau_p=500$ ns) using an XeF laser beam ($\lambda=0.352$ μm).

The 0.4-ns pulse experiments were conducted at the National Laser Users Facility, Laboratory for Laser Energetics, Rochester, New York. For those experiments, the frequency-tripled output of a glass laser ($\lambda=0.3513$ μm) was used to determine a laser breakdown threshold in 1 atm of argon. The pulse shape is shown in Fig. 9(a). The measurements indicated a threshold of $(6\pm4)\times10^{12}$ W/cm^2. The large error limits are the results of uncertainties in the beam spatial distribution at focus, as well as difficulties that were encountered in precisely defining the onset of "breakdown."

The long pulse ($\tau_p=500$ ns) experiments were carried out at our laboratory using an e-beam-pumped XeF laser (Maxwell Labs., Inc., Maximer^{TM} 10-1) that could deliver up to 6 J of energy when the full beam was used. The temporal pulse shape is shown in Fig. 9(b). The laser beam was focused by a 1.6-m focal-length aluminized mirror. The effective beam irradiated area in the focal plane was determined by attenuating the beam intensity by several orders of magnitude using neutral density filters and then recording the beam spot on photographic film. When focusing the full output beam (a geometric square 10 cm on a side with the center 5 cm$\times$5 cm square missing due to eclipsing by the output coupling mirror), it was found that the effective minimum spot size was approximately five to ten times that predicted for diffraction-limited focusing. Furthermore, upon close examination, the beam structure at focus was shown to consist of a complex interference pattern having a "feathered-like" appearance with several central "hot spots." Unable to determine the source of this "aberration" and to eliminate it, we decided to try to improve spatial coherence by masking the beam so that only a 2.5 cm$\times$2.5 cm segment was allowed to pass. The resulting focal plane beam profile was found to be well behaved and to possess the characteristic pattern and dimensions of the far field diffraction from a square aperture. For the 1.6-m focal-length mirror, the dimension of the central lobe in the focal plane (containing approximately 80% of the total power) was found to be 5×10^{-3} cm. The long pulse length experiments yielded a threshold for breakdown at atmospheric pressure of 3×10^{10} W/cm^2.

We have recently carried out a series of experiments at the Massachusetts Institute of Technology—National Science Foundation (MIT/NSF) Regional Laser Laboratory. The experiments were carried out using the laboratory's Molectron MY-34 high-power pulsed Nd:YAG laser. This laser is used to generate high-intensity visible and ultraviolet light through second, third, and fourth harmonic generation. For the present studies, breakdown measurements were performed using only the second and third harmonics ($\lambda=0.53$ and 0.35 μm). The gases for which we have obtained data include argon, neon, nitrogen, and xenon. We report here only the results for argon at 0.35

μm (results for other gases will be presented elsewhere). The pulse energy was 0.125 J and the pulse duration 15 ns (full width at half maximum). Under normal operation, the oscillator operates over several axial modes and the resulting temporal waveform displays several prominent "beats," with the separation between beats being the cavity round-trip transit time of 7 ns. A typical temporal waveform is shown in Fig. 9(c). The output beam spatial intensities profile is Gaussian and the beam is specified as uniphase. The $1/e^2$ beam diameter at the exit of the laser is ~ 8 mm.

For the experiments at MIT, focusing was performed using transmissive optics of 7.5, 20, and 30 cm. For the majority of the measurements only the central core of the beam was used ($r \leq 1/e$ beam waist). This ensured a high degree of spatial coherence within the beam and made lens aberrations negligible due to the large f/numbers used (f/numbers > 10). Beam focusing under these conditions was very nearly diffraction limited. The intensity at focus was varied by (a) apodizing the beam before the lens and (b) varying the laser pump energy. Beam energy (or power) transmitted through the focus was measured using a 1-cm^2 Laser Precision pyroelectric joulemeter (or a 2.5-cm-diameter Scientech laser power meter). The experimental configuration is shown in Fig. 10.

For all the experiments carried out by us ($\tau_p = 0.4$, 15, and 500 ns) breakdown threshold was defined as the laser power density at which (1) measurable attenuation ($\geq 10\%$) of the transmitted beam was observed and (2) a "bright" visible glow was seen in the laser focal region.

We show in Fig. 11 the experimental data, which was plotted as $I_{\rm th}$ versus τ_p, where $I_{\rm th}$ is the threshold intensity on axis. The data of Buscher *et al.* and of Alcock *et al.* were raised by a factor of 2, since the data that they quoted corresponded to intensity averaged over the focal area.

In order to compare our model with the data, we have made a series of calculations at varying laser fluxes using the early- and late-time breakdown models discussed in Secs. II and III. The breakdown time was defined as $\tau_{\rm br} = t_1 + t_2$, where t_1 is the time required to bring the electron number density to 10^{13} cm^{-3} using the early-time model and t_2 the time required to increase the density by another factor of 10^4 using the late-time model. Assuming a constant intensity pulse, we obtain the curve shown

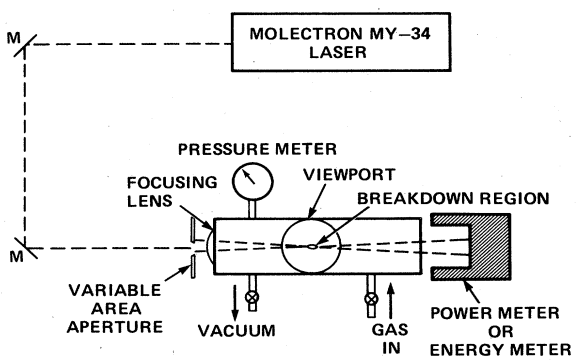

FIG. 10. Experimental configuration.

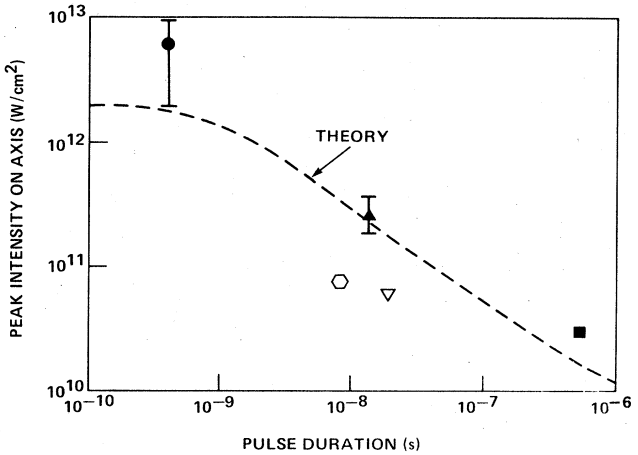

FIG. 11. Experimental and theoretical breakdown thresholds in argon at $p = 1$ atm as a function of pulse length. ●, Ref. 7, $\lambda = 351$ nm; ▲, this work, $\lambda = 355$ nm; ■, Ref. 7, $\lambda = 353$ nm; ○, Ref. 12 raised by a factor of 2, $\lambda = 347$ nm; ∇, Ref. 6 raised by a factor of 2, $\lambda = 347$ nm.

in Fig. 11, for $p = 1$ atm. Agreement with our data is seen to be quite good. The data of Alcock *et al.* and Buscher *et al.*, however, are found to be a factor of 5 below our calculated values. We find that for $I > 3 \times 10^{11}$ W/cm^2 the early-time breakdown stage is dominated by MPI, which builds up the electron density to a value in excess of 10^{13} cm^{-3} in a time $t < \tau_p/10$. When $I > 2 \times 10^{12}$ W/cm^2, MPI alone is able to create 10^{17} e^-/cm^3 in the focal volume, and the threshold curve varies as $\tau_p^{-1/5}$. If we take into account diffusion losses, the comparison between theory and experiments at $\tau_p = 500$ ns is improved. The loss rate of electrons using a *free*-electron diffusion coefficient in argon $\mathscr{D} = 3000$ cm^2/s and a focal radius $a = 25$ μm is calculated to be $\nu_D = 2.4\mathscr{D}/a^2 \cong 10^9$ s^{-1}. In order to compensate for this loss rate, the avalanche rate must exceed 10^9 s^{-1}, which would require (see Fig. 4) $I > 5 \times 10^{11}$ W/cm^2. Diffusion becomes *ambipolar,* however, and the loss rate decreases by a factor of ~ 250 when the Debye length is comparable to the focal radius; this occurs at an electron density (for $kT_e = 1.5$ eV, $a = 25$ μm) $n_e = kT_e/(4\pi e^2 a^2) = 10^{11}$ cm^{-3}. The requirement that MPI generate this density in 50 ns ($= \tau_p/10$) will lead to a threshold $I_{\rm th} = 4 \times 10^{10}$ W/cm^2, which is very close to the experimental threshold.

We believe that the discrepancy between the observed threshold and the calculated one at $\tau_p = 0.4$ ns is very probably due to our *experimental* criterion for breakdown. Observation of a flash in the focal volume, accompanied by a measurable decrease ($> 10\%$) in transmitted energy, is associated with a significant degree of ionization in the whole focal volume. Our theoretical criterion of $n_e \cong 10^{17}$ e^-/cm^3 on axis at the end of the pulse would certainly not correspond to any measurable attenuation of the beam. Requiring complete ionization by the end of the pulse would raise the threshold by a factor of $250^{1/5} = 3$ and would yield $I_{\rm th} = 3 \times 10^{12}$ W/cm^2, in better agreement with the data. Also, the occurrence of the sharp onset of a flash is more indicative of a cascade-type breakdown

than MPI-induced breakdown. It is only at a flux in excess of 3×10^{12} W/cm^2 that the cascade growth time becomes smaller than the laser pulse time $\tau_p \sim 0.4$ ns.

V. SUMMARY AND DISCUSSION

We have analyzed in this paper the various physical mechanisms that lead to gas breakdown when argon is irradiated by a 0.35-μm laser pulse. The breakdown model that we developed includes electron generation by MPI and by electron-impact excitation of the gas followed by photoionization of excited states. We have separated the breakdown development into an early stage ($n_e < 10^{14}$ cm^{-3}) when electron-electron collisions are too slow to make the distribution function Maxwellian and a late-time stage where we included many more reactions involving recombination and argon dimer formation. The cascade growth rate α^+ in the early stage is shown in Fig. 4. α^+ can be represented as a function of Ip^m where m varies from 0.5 (high p, low I) to 1 (low p, high I). The cascade growth rate was found to increase by a factor of 2 at high n_e when the tail of the electron distribution function is readily populated by electron-electron collisions. At high electron densities, just before complete breakdown of the gas, one of the major absorption mechanisms was found to be photoionization of excited argon monomers formed by three-body electron-ion recombination. A new series of experimental breakdown thresholds in argon at 0.35 μm have been reported here. The measurements were carried out at the MIT/NSF Regional Laser Laboratory using their 15-ns frequency-tripled Nd:YAG laser. Agreement between experiments and theory was found to be very good (see Fig. 11). Though we believe that we have included the most important processes that determine the evolution of the breakdown, the accuracy of our results suffers from the numerical uncertainty of several important rate coefficients, namely the IB absorption coefficient, the rate of photoionization of the 4s states by absorption of two photons, and the MPI rate at 0.35 μm.

Several expressions for IB absorption have been derived in the literature[9,16–18] that relate the IB absorption coefficient K_a to the momentum-transfer cross section. Due to the presence of a Ramsauer minimum in the electron-argon elastic cross section, the momentum-transfer cross section is strongly dependent on electron energy (it varies by two orders of magnitude from $\epsilon=0.3$ to $\epsilon=3$ eV) and the IB absorption coefficient will vary depending on the expression used. We have used in this paper the expression derived by Dalgarno and Lane.[17] We have also numerically solved the quantum kinetic equation using the IB absorption coefficient of Phelps[9] and found the IB absorption rate to be a factor of ~2 smaller under similar conditions. A quantum-mechanical calculation of K_a in argon and in other monatomic gases has been carried out by Geltman[34] using a model atomic potential that was adjusted to fit experimental scattering cross sections. The shortest wavelength for which K_a has been calculated, however, was 0.53 μm. Using the sum of the matrix elements $|R^A_{l\pm1}|^2$ in Ref. 34, Eq. (11), provided to us by Geltman[35] to calculate K_a at several specific electron energies, we estimate from these calculations that K_a would be a factor of ~3 times larger than that used in this paper. This would lead, at high laser intensities when $\alpha^+ \simeq (k_1+k_2)n \propto K_a$ [see discussion after Eq. (5)], to a cascade rate in the early-time breakdown model three times larger than that plotted in Fig. 3. The cascade rate in the late-time breakdown stage, when electron-electron collisions are effective in populating the tail of the electron distribution function, is not affected as much, however, since this cascade rate is already a factor of 2 larger than in the early-time cascade development.

Photoionization of excited states plays an important role in breakdown at 0.35 μm. It is for this reason that breakdown calculations using wavelength scaling of microwave breakdown results would yield erroneous results, even at low intensities (where multiphoton ionization from the ground state of Ar is unimportant). For example, the breakdown threshold in argon at 10.6 μm for $p=1$ atm, $\tau_p=80$ ns is 8×10^8 W/cm^2, corresponding to a scaled threshold at 0.35 μm of 10^{12} W/cm^2, while the actual threshold is 8×10^{10} W/cm^2 (neglecting diffusion losses), i.e., more than a factor of 10 lower. The lowest-lying excited states of argon lie within $2h\nu$ of the ionization continuum and two-photon ionization of these states plays an important role in the breakdown process. We have estimated the cross section for absorption of two photons and calculate that at 10^{10} W/cm^2 the lifetime of the 4s states is 10^{-7} s and decreases to 10^{-9} s at 10^{11} W/cm^2. We have estimated the photoionization rate W_{ml} (Appendix B) assuming that there is no constructive or destructive interference between terms involving different intermediate states. If constructive interference occurs, the rate may be up to 4 times larger than quoted in the paper.

The multiphoton ionization rate that we used was inferred from the breakdown data of Kracyuk and Pashinin and, for lack of information, we had to make certain assumptions on the experimental condition under which a "faint glow" was observed (distance of observer from focus, dark adapted eye). We estimate that the cross section that we have derived [Eq. (8)] is accurate to within a factor of better than 10. This would lead to a breakdown threshold uncertainty based on MPI alone of $\pm60\%$ (equivalent to a factor of $10^{1/5}$).

The principal channel for laser energy deposition in the gas was found to be photoionization of states formed by three-body recombination. We treated the rate of energy deposition as if three-body recombination were the rate-limiting step. At low intensities ($I < 10^9$ W/cm^2) and high electron densities ($n_e > 10^{17}$ cm^{-3}), however, three-body recombination may be fast enough so as to maintain a Boltzmann distribution of excited states. Absorption should then be treated by calculating photoionization using an equilibrium population of excited states. There will nevertheless always be, for a given I, an n_e where photoionization and three-body recombination rates are equal. The theory of Pitaevskii which yields the three-body recombination rate μ given by Eq. (34) is based on a model for diffusion of (bound) electrons in energy space through collisions of highly excited atoms with free electrons, there being a tendency on each collision for the bound electron to become more tightly bound until it can

radiatively fall to a low-lying or ground state. Since photoionization of excited states, under a high-intensity pulse, will provide a *sink* for (bound) electrons that are much more weakly bound than in Pitaevskii's model, it is reasonable to assume that the recombination rate in the presence of a laser field is larger than that given by Eq. (34). A proper analysis of recombination in the presence of a high-intensity laser field remains, however, to be done.

We have not considered in our analysis the effect of gas expansion during the pulse, nor analyzed the effect of diffusion of ionized species out of the focal volume. Both effects should be included in a realistic and quantitative calculation of energy deposition for a given experimental configuration. When calculating breakdown threshold, however, one can usually neglect gas expansion in the case of cascade-dominated breakdown, since practically all the energy is deposited during the last e folding of electron density, which occurs during only a small fraction of the laser pulse. Expansion should play a more important role when breakdown by MPI dominates.

As was discussed in Sec. V the experimental and theoretical results are in good agreement, if one excludes the data taken at the frequency-doubled ruby laser beam wavelength. These last data are a factor of 5 lower than the model predicts (see Fig. 11). We cannot explain this discrepancy within the framework of our theoretical model. One may argue that nonlinear effects such as self-focusing may result in regions of high field amplitude where breakdown would occur on a faster time scale. Alcock *et al.* have observed self-focusing on their beam during the breakdown process. Self-focusing may occur when the population of excited states is high enough to affect the third-order polarizability. It is not expected, however, to play a role during the early-time breakdown phase which dominates the induction time to breakdown.

ACKNOWLEDGMENTS

We acknowledge useful discussion with L. Piper concerning the late-time chemistry in argon. We would like to express our gratitude to Mr. Steven Schertzer for his able assistance in carrying out the experiments and to the staff of the MIT Regional Laser Center for their hospitality. This work was supported in part by the Air Force Office of Scientific Research under Contract No. F49620-83-C-0039 and in part by the U.S. Defense Advanced Research Projects Agency under Contract No. N00014-78-C-0328.

APPENDIX A: EVALUATION OF MPI CROSS SECTION IN ARGON

Kracyuk and Pashinin[11] observed breakdown in Ar at atmospheric pressure under the laser conditions $I=5\times10^{11}$ W/cm^2, $\tau_p=30$ ps. We can obtain an estimate of the multiphoton ionization cross section from their data as follows. Let the cross section Q be defined by

$$\frac{dn^+}{dt}=Q\Phi^5 n\ ,$$

where Φ is the photon flux in cm^{-2}s^{-1}. A faint glow corresponds to $\cong 100$ photons reaching the eye. If $V_{\rm eff}$ is the effective focal volume, n the gas density, and δ the degree of ionization, the number of photons reaching the eye is $\cong n\delta V_{\rm eff}\Omega$, where Ω is the solid angle subtended by the eye. We have assumed one visible photon emitted per recombination event.

The effective focal volume is

$$V_{\rm eff}=\frac{\int I^5(\mathbf{r})d^3r}{I_{\rm max}^5}\ . \tag{A1}$$

If we assume that the beam has a diffraction limited Gaussian profile near focus, then

$$I(\mathbf{r})=I(r,z)=\frac{I_{\rm max}}{1+\left[\frac{\lambda z}{\pi W_F^2}\right]^2}\exp\left[-\frac{2r^2}{W_F^2\left[1+\left[\frac{\lambda z}{\pi W_F^2}\right]^2\right]}\right], \tag{A2}$$

where W_F is the $1/e^2$ beam radius at focus and z the axial distance from the geometric focal point.[36] Integration over $\mathbf{r}$ then yields

$$V_{\rm eff}=\frac{1}{32}\frac{\pi^3 W_F^4}{\lambda}\ . \tag{A3}$$

The focal area at half-intensity in Kracyuk and Pachinin's experiment was 1.4×10^{-5} cm^2, which leads to a value for W_F of 42 μm. Letting $\lambda=0.35$ μm in Eq. (A3), we obtain $V_{\rm eff}=8\times10^{-6}$ cm^3. We estimate under the conditions of the experiment (dark adapted eye, 1 m from the focal region) that $\Omega=\pi\times(0.3\text{ cm})^2/(100\text{ cm})^2=3\times10^{-5}$ sr. Finally, the experiments were performed near atmospheric pressure so that $n\cong 2\times10^{19}$ cm^{-3}. Therefore,

$$\delta=\frac{100}{nV_{\rm eff}\Omega}=\frac{100}{(2\times10^{19})(8\times10^{-6})(3\times10^{-5})}$$
$$=2\times10^{-8}\ .$$

At the end of the pulse $n^+/n=\delta=Q\phi^5\tau_p$, so that for $\phi=9\times10^{29}$ cm$^{-2}s^{-1}$ ($I=5\times10^{11}$ W/cm^2) and $\tau_p=3\times10^{-11}$ s, we have $Q=1\times10^{-147}$ cm^{10}s^4.

APPENDIX B: EVALUATION OF THE PHOTOIONIZATION RATE W_{ml}

We estimate in this appendix the rate of ionization of the 4s excited states in argon by absorption of two 3.5-eV photons. The transition rate for two-photon absorption is obtained from second-order perturbation theory with the interaction Hamiltonian

$$\Delta H=\frac{-e}{mc}\mathbf{A}_0\cdot\mathbf{p}\cos(\omega t)=e\mathbf{E}_0\hat{\mathbf{e}}\cdot\mathbf{r}\cos(\omega t) \tag{B1}$$

with $\mathbf{A}_0\cos(\omega t)$ and $\mathbf{E}_0\cos(\omega t)$ the vector potential and electric field of the electromagnetic wave, respectively. The unit vector $\hat{\mathbf{e}}$ is the polarization vector which we take

to be in the **x** direction. The transition rate between the lower state (m) and the upper (continuum) state (l) is[37]

$$W_{ml}=\frac{\pi}{8\hbar^2}\int\rho(2\omega+\omega_m)\left|\sum_j\frac{\Delta H_{lj}\Delta H_{jm}}{(\omega-\omega_{jm})}\right|^2 d\Omega\ . \tag{B2}$$

The integration is carried over solid angle Ω, ρ being the density of final states (per unit ω) and $\omega_{jm}=(E_j-E_m)/\hbar$. The sum is over all intermediate states of energy E_j.

We first evaluate Eq. (B2) under the condition where only one intermediate state j is predominant in the sum. We use the **r** representation of the interaction Hamiltonian to evaluate the matrix element between the two bound states m and j and the **p** representation between the bound state and the free state. Using the fact that $|\mathbf{E}_0|=(\omega/c)|\mathbf{A}_0|$, we obtain

$$W_{ml}=\frac{\pi}{8\hbar^4}\frac{\rho(2\omega+\omega_m)}{(\omega-\omega_{mj})^2}\frac{e^4E_0^4\hbar^2}{m^2\omega^2}\int d\Omega\, x_{mj}^2\left|\left\langle\psi_j\frac{\partial}{\partial x}\psi_l\right\rangle\right|^2 . \tag{B3}$$

We can express the matrix element x_{mj} in terms of the oscillator strength, f_{mj} of the transition

$$x_{mj}^2=\frac{\hbar}{2m\omega}f_{mj}\ . \tag{B4}$$

The other matrix element can be related to the photoionization cross section of the intermediate state. From Bethe and Salpeter the cross section is[38]

$$\sigma_{\rm phi}=\frac{2\pi e^2\hbar^2}{m^2c\nu}\left|\int u_{n'}^*\left[\sum_j e^{i\mathbf{k}\cdot\mathbf{r}_i}\frac{\partial u_n}{\partial x_i}\right]d\tau\right|^2 , \tag{B5}$$

where $\mathbf{r}_i$ is the position of the ith electron, $\nu=\omega/2\pi$, and the integral extends over the configuration space of all electrons. The wave functions ψ_n are normalized per unit energy interval, while the wave functions in Eq. (B5) are normalized per unit volume. We thus have

$$u_n=\psi_n\left[\frac{\rho(\omega_n)}{\hbar}\right]^{1/2} . \tag{B6}$$

Combining Eqs. (B3)—(B6) we obtain ($I=cE_0^2/8\pi$)

$$W_{ml}=\frac{\pi e^2}{(\hbar\omega)^2(\omega-\omega_{jm})^2mc}I^2\sigma_{\rm phi}f_{mj}\ .$$

Expressing I in W/cm^2, $\sigma_{\rm phi}$ in cm^2, and energies in eV, we obtain

$$W_{ml}=\frac{5\times10^5I^2\sigma_{\rm phi}f_{mj}}{(h\nu)^2(h\nu-\epsilon_{jm})^2}\ . \tag{B7}$$

A tabulation of ϵ_{jm} and f_{mj} for allowed transitions can be found in Ref. 23. We have reproduced in Table I the states that contribute the most to the sum in Eq. (B2). The contribution is large either because there is a near resonance $\epsilon_{jm}\cong h\nu$ or because f_{mj} is large. The ionization cross section $\sigma_{\rm phi}$ can be estimated from the relation[39]

$$\sigma_{\rm phi}=7.91\times10^{-18}\frac{n}{Z^2}\left[\frac{\nu_n}{\nu}\right]^3 {\rm cm}^2 , \tag{B8}$$

where ν_n is the frequency at the photoionization edge, ν the photon frequency, Z the ionic charge, and n the principal quantum number of the state j. The quantity $[\sigma_{\rm phi}f_{jl}/(h\nu-\epsilon_{jm})]$ is shown in the last column of Table I. One sees that the near-resonant states contribute insignificantly to the sum since f_{mj} and $\sigma_{\rm phi}$ are both small.

We see from Table I that for each s state considered there are N (=4) intermediate states that contribute about equally to the integrand in Eq. (B2). We can estimate the overall effect of these N states, neglecting subtle interference effects, by considering the problem as being analogous to finding the modulus of the sum of N complex vectors having the same length but random orientation in the complex plane. The total rate would then be evaluated by summing the rates W_{ml} given by Eq. (B7) over the N states (i.e., neglecting cross terms that on average cancel). We thus obtain the following estimate of the photoionization cross section for $h\nu=3.5$ eV:

$$W_{ml}=1.1\times10^{-13}I^2({\rm W/cm}^2)\ {\rm s}^{-1}\ . \tag{B9}$$

The above formula predicts a lifetime of the 4s state of 10^{-8} s at 10^{10} W/cm^2, 10^{-9} s at 3×10^{10} W/cm^2, and 10^{-10} s at 10^{11} W/cm^2.

[1] C. Grey Morgan, Rep. Prog. Phys. **38**, 621 (1975).

[2] A. D. MacDonald, *Microwave Breakdown in Gases* (Wiley, New York, 1966), p. 188.

[3] E. Yablonovich, Appl. Phys. Lett. **23**, 121 (1973).

[4] H. Cohn, M. Hacker, B. Lax, and W. Halverson, J. Appl. Phys. **46**, 668 (1974).

[5] Ya. B. Zel'dovich and Yu. P. Raizer, *Physics of Shock Waves and High Temperature Hydrodynamic Phenomena, Vol. 1* (Academic, New York, 1966), p. 259. Note, however, that during the early stages of the breakdown process, the electron distribution function is not Maxwellian and one cannot, truly speaking, talk of an electron temperature. The temperature to use in the formula for the IB absorption coefficient is $\frac{2}{3}\langle\epsilon\rangle$ where $\langle\epsilon\rangle$ is the average electron energy. At wavelengths longer than 1.06 μm one can approximate $[1-\exp(-hc/\lambda kT)]$ by $hc/\lambda kT$. This leads to a threshold varying as λ^{-2}, which is the wavelength scaling that is usually mentioned in the literature.

[6] A. Buscher, R. Tomlinson, and K. Damon, Phys. Rev. Lett. **15**, 847 (1965).

[7] G. Weyl, D. Rosen, J. Wilson, and W. Seka, Phys. Rev. A **26**, 1164 (1982).

[8] C. Friedland, Phys. Rev. A **12**, 2024 (1975).

[9] A. V. Phelps, in *Physics of Quantum Electronics*, edited by P. L. Kelley *et al.* (McGraw-Hill, New York, 1966), p. 538.

[10] Ya. Zel'dovich and Yu. Raizer, Zh. Eksp. Teor. Fiz. **47**, 1150 (1964) [Sov. Phys.—JETP **20**, 772 (1965)].

[11] I. Krasyuk and P. Pashinin, Pis'ma Zh. Eksp. Teor. Fiz. **15**, 471 (1972) [JETP Lett. **9**, 354 (1969)].

[12] A. Alcock, K. Kato, and M. Richardson, Opt. Commun. **6**, 342 (1972).

[13] P. Lambropoulos, Adv. At. Mol. Phys. **14**, 87 (1977).

[14]C. Lecompte, G. Mainfray, C. Manus, and F. Sanchez, Phys. Rev. A **11**, 1009 (1975).
[15]G. Mainfray (private communication). The coherence time for a multimode laser beam is the same as the time duration of the spike obtained through modelocking, i.e., 10—100 ps, if the same number of modes are oscillating.
[16]Ya. Zel'dovich and Yu. Raizer, Zh. Eksp. Teor. Phys. **47**, 1150 (1964) [Sov. Phys.—JETP **20**, 772 (1965)].
[17]A. Dalgarno and N. Lane, Astrophys. J. **145**, 623 (1966).
[18]N. Kroll and K. Watson, Phys. Rev. A **5**, 1883 (1972).
[19]E. Eggarter, J. Chem. Phys. **62**, 833 (1974).
[20]J. Jacob and J. Mangano, J. Appl. Phys. **79**, 467 (1976).
[21]M. Shaper and H. Scheibner, Beitr. Plasmaphys. **9**, 45 (1969).
[22]R. Center (unpublished).
[23]M. Wiese, M. Smith, and B. Miles, *Atomic Transition Probabilities, Vol. II: Sodium Through Calcium,* Natl. Bur. Stand. Ref. Data Ser., Natl. Bur. Stand. (U.S.) Circ. No. 22 (U.S. GPO, Washington, D.C., 1969).
[24]L. Frost and A. Phelps, Phys. Rev. A **136**, 1538 (1964).
[25]D. Rapp and P. Englander-Golden, J. Chem. Phys. **43**, 1464 (1965).
[26]L. Spitzer, *Physics of Fully Ionized Gases* (Wiley, New York, 1962), p. 133.
[27]Y. Shiu and M. Biondi, Phys. Rev. A **17**, 868 (1978).
[28]D. Lorentz and R. Olsen, Stanford Research Institute (Menlo Park, CA 94025) Report dated Nov. 27, 1972, Contract No. N00014-72-C-0457 (unpublished).
[29]A. Gurevich and L. Pitaevskii, Zh. Eksp. Teor. Phys. **46**, 1281 (1964) [Sov. Phys.—JETP **19**, 870 (1964)].
[30]D. Bates, A. Kingston, and R. McWhirter, Proc. R. Soc. London Ser. A **267**, 297 (1962).
[31]Reference 5, p. 390.
[32]Reference 5, p. 407.
[33]Reference 5, p. 271.
[34]S. Geltman, J. Quant. Spectrosc. Radiat. Transfer **13**, 601 (1973).
[35]S. Geltman (unpublished).
[36]D. Marcuse, *Light Transmission Optics* (Van Nostrand, New York, 1977), p. 232.
[37]A. Yariv, *Quantum Electronics* (Wiley, New York, 1967), p. 358.
[38]H. Bethe and E. Salpeter, *Quantum Mechanics of One and Two Electron Atoms* (Academic, New York, 1957), p. 296.
[39]Ya. B. Zel'dovich and Yu. P. Raizer, *Physics of Shock Waves and High Temperature Hydrodynamic Phenomena, Vol. 1* (Academic, New York, 1966), p. 265.